THE INTERNATIONAL JOURNAL OF MEDICAL ROBOTICS AND COMPUTER ASSISTED SURGERY
Int J Med Robotics Comput Assist Surg 2008; **4**: 180–191.
Published online 24 April 2008 in Wiley InterScience (www.interscience.wiley.com). **DOI:** 10.1002/rcs.184

ORIGINAL ARTICLE

Three-dimensional ultrasound-guided robotic needle placement: an experimental evaluation

Emad M. Boctor,[1]
Michael A. Choti,* [2]
Everette C. Burdette[3] and
Robert J. Webster III[4]

[1]*Department of Radiology, Johns Hopkins Medical Institute, Baltimore, MD, USA*

[2]*Department of Surgery, Johns Hopkins Medical Institute, Baltimore, MD, USA*

[3]*Acoustic MedSystems Inc., Urbana-Champaign, IL, USA*

[4]*Department of Mechanical Engineering, Vanderbilt University, Nashville, TN, USA*

*Correspondence to:
Michael A. Choti, Johns Hopkins Medical Institutions, Department of Surgery, 600 North Wolfe Street, Halsted 610, Baltimore, MD 21287, USA. E-mail: mchoti@jhmi.edu

Accepted: 25 January 2008

Abstract

Background Clinical use of image-guided needle placement robots has lagged behind laboratory-demonstrated robotic capability. Bridging this gap requires reliable and easy-to-use robotic systems.

Methods Our system for image-guided needle placement requires only simple, low-cost components and minimal, entirely off-line calibration. It rapidly aligns needles to planned entry paths using 3D ultrasound (US) reconstructed from freehand 2D scans. We compare system accuracy against clinical standard manual needle placement.

Results The US-guided robotic system is significantly more accurate than single manual insertions. When several manual withdrawals and reinsertions are allowed, accuracy becomes equivalent. In *ex vivo* experiments, robotic repeatability was 1.56 mm, compared to 3.19 and 4.63 mm for two sets of manual insertions. In an *in vivo* experiment with heartbeat and respiratory effects, robotic system accuracy was 5.5 mm.

Conclusions A 3D US-guided robot can eliminate error bias and reduce invasiveness (the number of insertions required) compared to manual needle insertion. Remaining future challenges include target motion compensation.

Keywords 3DUS; medical robots; IGT; CIS; liver; ablation; RFA

Introduction

Needles are one of the least invasive and most frequently used interventional tools, applicable in nearly every area of the body. Treatment efficacy in needle-based procedures is strongly dependent on the accuracy of tip placement. Specifically, biopsies inadvertently taken from the wrong locations can result in clinically significant false negatives. Conventional free-hand needle placement involves simultaneous manipulation of the ultrasound (US) probe and needle while the physician mentally relates images on a video screen to locations inside the patient. The fact that physicians are accurate enough to satisfy some clinical objectives using this challenging manual procedure is a testament to their dedication, training and skill. However, the two-dimensional (2D) nature of imaging and dependence on operator skill limit the consistency and effectiveness of treatments delivered with this manual procedure (1). Robotic systems are an appealing alternative able to perform spatial registration and manipulation tasks rapidly, accurately and repeatably. Because of this, needle placement robots have garnered substantial interest within the research community in

recent years, and many innovative systems and algorithms have been developed [see (2) as an example of a complete system and (3) for an overview]. While the excellence of robots at needle placement has been well established, widespread clinical adoption of needle placement robots has not immediately followed. One reason for this is that contemporary medical robotic systems often introduce a prohibitively complex engineering entourage into otherwise rather straightforward needle placement procedures.

This paper describes the experimental evaluation of an image-guided robotic needle placement system designed to reduce the cost, complexity and calibration time of such systems, thereby enhancing their utility in challenging real-world surgical environments. This system uses intraoperative US imaging for image guidance, an attractive solution because of its wide availability and low cost. We build three-dimensional (3D) intraoperative US volumes from 2D slices to provide an improved environment for surgical planning and to enhance accuracy in the coronal plane, which is often difficult or impossible to view on 2D images, due to anatomical constraints. Our system then applies algorithms designed to achieve accurate robotic needle placement while streamlining calibration and registration procedures. While the various parts of our image-guided surgery system have been shown to function well individually (4–7), this paper considers an experimental evaluation of our complete, fully integrated system in comparison with current clinical standard free-hand techniques in order to demonstrate clinical utility. To the best of our knowledge, this represents the first direct accuracy and repeatability comparison between manual and image-guided robotic needle insertion. While this work is applicable to many kinds of needle-delivered therapies and diagnoses throughout the body, our motivating example is thermal treatment of liver lesions. Liver cancer treatment is an excellent proving ground for our system because of the high potential impact of improved needle tip accuracy on clinical outcomes.

Medical motivation: Liver Cemca Therapy

Despite recent advances in cancer therapy, treatment of primary and metastatic tumours of the liver remains a significant challenge in health care worldwide. Hepatocellular carcinoma (HCC) is one the most common malignancies encountered throughout the world, causing over 1 million deaths annually (8,9), and 5 year survival rates are only 5–12% (47). Metastatic liver cancer from a variety of other primary malignancies is also a common health problem and colorectal metastases are the most common hepatic malignancy in the USA (10).

Potentially curative treatment options for primary and secondary liver cancer include surgical resection and in some cases liver transplantation, but only a small percentage of patients are candidates, due to additional health problems, age, tumour location and number, etc. Interstitial ablative approaches offer an alternative for many otherwise untreatable patients, and have been a topic of significant recent interest in the research community. Approaches include chemical ablation, cryoablation (11) and radiation therapy (12), but perhaps the most promising is thermal ablation, using energy sources such as radiofrequency (RF) (13,14), microwave (15) or focused ultrasound (16,17).

These thermal approaches generally require placing the probe tip at specific target location(s) in the liver parenchyma. In the case of RF ablation (Figure 1), heat created around each of several electrodes causes coagulative necrosis. Local tissue ablation thus increases the number of patients eligible for potentially curative therapy, is performed with lower morbidity than resection, and can be employed minimally invasively.

Related work

US imaging is a widely used guidance modality for medical interventions. It is portable, interactive, real-time, safe, cost-effective and convenient to use in outpatient clinics. Significant research has been dedicated to using US for image-guided therapy (IGT), but technical improvements are needed before the full potential of US can be realized in IGT. An important advancement has been the assembly of individual 2D US images into 3D volumes (18), which can be used for IGT by relating the position of surgical tools to the 3D US.

Developing of a flexible US IGT system for liver ablation or other applications requires integrating: (a) real-time simultaneous tracking of both the ultrasound probe and the ablation tool; (b) ablation planning software; (c) 3D ultrasound visualization; and (d) a robot control interface, if a robot is used to manipulate the ablation needle. For example, Stradx (19) and In-Vivo (20) offer tracked 3D US systems with visualization, but these

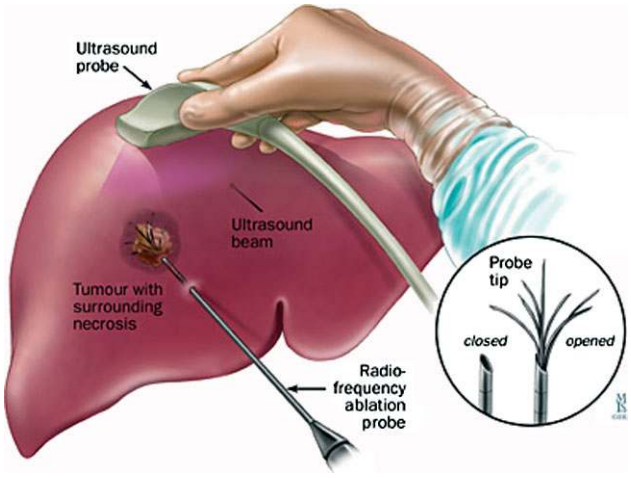

Figure 1. Typical radiofrequency ablation of a liver tumour guided by freehand 2D US. Image courtesy of the Johns Hopkins University Liver Cancer Center

DOI: 10.1002/rcs

are not open systems, creating technological, logistical and even legal challenges for researchers who wish to create a US-based IGT system. Despite these difficulties, there have been some successes in doing so, including MISON (46), an intraoperative imaging system that integrates 3D US and navigation in neurosurgery. A primary goal of the MISON system is to compensate for the deformation of the brain after opening the skull, and the system includes tracked tools but no robotic components. Prostate brachytherapy systems also routinely use US (21–25), but these are also closed systems that cannot be easily adapted to new clinical objectives, such as liver cancer treatments. Although these examples illustrate the feasibility and importance of US in IGT, a standard and open environment for the development of US-guided therapy has not yet been produced, and is necessary to facilitate innovative US IGT applications throughout the body.

The system that is the subject of the experiments presented in this paper is intended to fill this gap by introducing an open-source platform to develop various specialized US IGT systems using real-time 2D and/or 3D US imaging (26). Under the title, 'Computer-integrated Surgery Guided by US Imaging' (CISUS), our software is currently being integrated into the 3D Slicer (45), an open source research tool intended for diagnostic visualization and surgical planning. The software also enables direct control of robotic systems for image-guided needle placement. In addition to CISUS, our group has developed related software for automatic ultrasound calibration. This toolkit, 'UltraCal', has been successfully used in many ultrasound research projects at Johns Hopkins (27).

The challenge for the robotic component of our system is to align the needle with the desired entry trajectory and translate it to the entry site in a safe, practical and affordable manner. There are a variety of available methods for robotic needle manipulation, which are surveyed in (7). These include using general serial linkages as well as kinematically decoupled robots that create a mechanically enforced remote centre of motion (RCM) that coincides with the needle tip. Independent of the particular robot used, the workflow in an image-guided robotic needle placement system is generally: (a) register the robot to the imager; (b) select the target and entry points; (c) solve inverse kinematics; (d) move the needle to the entry point; (e) align the needle with the entry vector; and (f) insert the needle. Depending on the number of actuated degrees of freedom (DOFs) available, some steps may be executed manually without changing the workflow.

Obstacles that must be overcome in using robots to achieve this workflow in the operating room include reducing robot cost, increasing the speed of system set-up and operation and streamlining calibration procedures. In laboratory settings, it is also important to be able to rapidly adapt a given manipulator to hold new kinds of surgical tools. All of these factors are addressed by the virtual RCM algorithm (7), which we briefly outline below.

Materials and Methods

Our image-guided robotic needle placement system consists of three basic components: (a) a robot that employs virtual RCM control (7) to manipulate the needle; (b) the imaging system that reconstructs 3D US from 2D scans (5,6,28); and (c) integration software built on 3D Slicer that enables planning and visualization, and commands robot motion (5,6). We describe each of these components below, after discussing the motivation for the components and structure of our system.

System architecture

In contrast to previous work that used robots to manipulate both US probe and needle (6), we use a robot for needle manipulation only and do not require a robot for US acquisition. Our 3D US reconstruction algorithms are robust to the variability of manually collected images, even for a novice user. However, aligning the needle requires considerable precision and accuracy, which is facilitated by a robot. To enable 3D reconstruction from 2D US images, we track the US probe using an electromagnetic tracking system, which senses poses of the US probe when images are captured. We use the same tracking system to sense robot (needle) poses, placing the needle and images in a common reference frame. This facilitates virtual RCM control, removing the need for a separate procedure to register the robot with the imager, and streamlining calibration.

Figure 2 demonstrates the schematic architecture of our system, which includes:

- A PC-based surgical workstation providing overall application control, 2D and 3D US processing and surgeon interfaces.
- A conventional 2D ultrasound system (SSD-1400 ultrasound machine, Aloka Inc.).
- A five-DOF robot, composed of three prismatic and two rotational joints, for positioning the needle.
- An electromagnetic (EM) tracking system (Flock of Birds, Model 6D, Ascension Technology Inc.).

The EM base unit is fixed to the operating table, and individual sensors are attached to the US probe and needle holder.

Virtual RCM robot control

The virtual RCM (4,7) is a control algorithm for needle placement robots that aligns the needle with the insertion vector from the body entry point to the target within the liver. It requires minimal calibration and relaxes structural requirements on the robot used to manipulate the

DOI: 10.1002/rcs

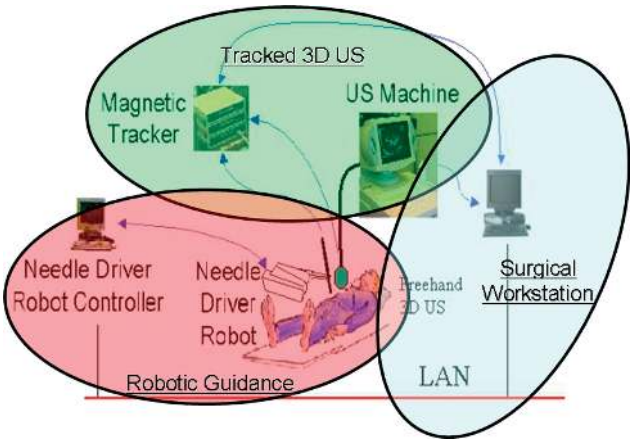

Figure 2. System components of our 3D US-guided robotic needle placement system. The system uses a tracked manual US probe and a robotic arm to manipulate the needle

needle, while permitting passive, unencoded positioning arms in the kinematic chain. These can be useful for preoperative gross positioning in the operating room. The tracking associated with the virtual RCM also removes the need for preoperative registration, decreasing system set-up time. Designed for accuracy, robustness and fast convergence, the virtual RCM consists of an artificial intelligence-based incremental adaptive motion cycle, accomplishing its objectives without requiring inverse kinematics, mechanical RCM enforcement or even encoding of joints. The following is a brief outline of the algorithm.

The virtual RCM is designed for use with a robot that consists of three linearly independent prismatic stages and two revolute stages. It requires two pieces of information obtained by preoperative calibration procedures: the transformation between the tracker and the needle tip frame, and the directions of motion of the prismatic stages. The former is readily obtained using a version of the well-known pivot calibration (28), and the latter is easily and quickly determined by moving the linear stages arbitrarily (maintaining a safe distance from the patient) while recording sensor readings. If the stages are orthogonal (as they are in our experimental system), direction cosines yield the desired rotation matrix.

The two-revolute DOF may in principle be included anywhere in the kinematic chain, but in practice will often consist of a two-DOF motorized rotational 'wrist' stage. In the system used in the experiments presented here, we use a wrist stage (29) designed to provide a mechanically constrained RCM. However, as discussed in (7), the virtual RCM is designed to enable the use of generic wrists that may be easier to construct and calibrate than existing RCM stages. We demonstrate this in our experimental system by including a tool holder that purposely removes the mechanical RCM property of the wrist by holding the needle off the RCM point. Because the tool is not on a mechanically constrained RCM, the yaw and pitch (α and β) DOFs of the wrist are not decoupled, and thus cannot be optimized individually to align the needle (see Figure 3), as would normally be done in mechanically constrained RCM systems.

To align the needle, the virtual RCM applies a heuristic search to simultaneously optimize α and β angles to align the needle with the desired entry vector. It begins by discretizing each rotational DOF and partitioning the search space into two subspaces, one for each angle. A heuristic function (the cross-product between the needle and the desired entry vector) then guides the search to optimize needle alignment. In practical terms, this means that the robot makes incremental motions, and after each it checks to determine whether the needle is becoming more or less aligned. This tells the robot which direction is likely to cause better alignment. By alternately moving the angles in small steps, the robot is able to rapidly servo to the proper alignment.

Each small angular motion will also result in some translation of the needle tip. However, we maintain the tip on a 'virtual RCM' point by immediately compensating for this translation (sensed by the tracker), using the linear stages after each incremental angular motion. We note that this algorithm is also applicable to other imaging modalities besides US. All that is necessary is to determine the pose of a point on the tool holder. This can be achieved by including various fiducials that can be seen in images, e.g. the z-frame fiducial, which enables pose extraction from a single CT slice (30).

The virtual RCM algorithm addresses cost and speed without sacrificing accuracy, enabling use of robots that are mechanically simple and are permitted to have unknown transformations (e.g. passive positioning arms) in their kinematic chains. Ease of use is improved by combining tracking or fiducial-enabled, image-based sensing of tool pose with our algorithm that nearly eliminates calibration requirements. The algorithm is applicable when the tool does not lie on a mechanically constrained fulcrum, enabling rapid retrofitting of existing robots to manipulate new tools (e.g. multiple kinds of needles, radiofrequency ablation probes, steerable needles, etc.), and use of robots that do not have a mechanically constrained RCM.

Freehand tracked 3D US

The freehand tracked US system entails compounding acquired 2D US images into a 3D volume. This provides a tool for intraoperative planning. Tracking the US probe handle (along with the spatial calibration discussed below) identifies the location and orientation of each 2D scan. The main components of a freehand tracked 3D US system are:

- The *acquisition and synchronization module*, which simultaneously captures synchronized US and tracker information and sets the parameters of both units.
- The *reconstruction module*, which converts the scattered arrays of images into a structured 3D voxel array. This is done by a user-selected algorithm, with

DOI: 10.1002/rcs

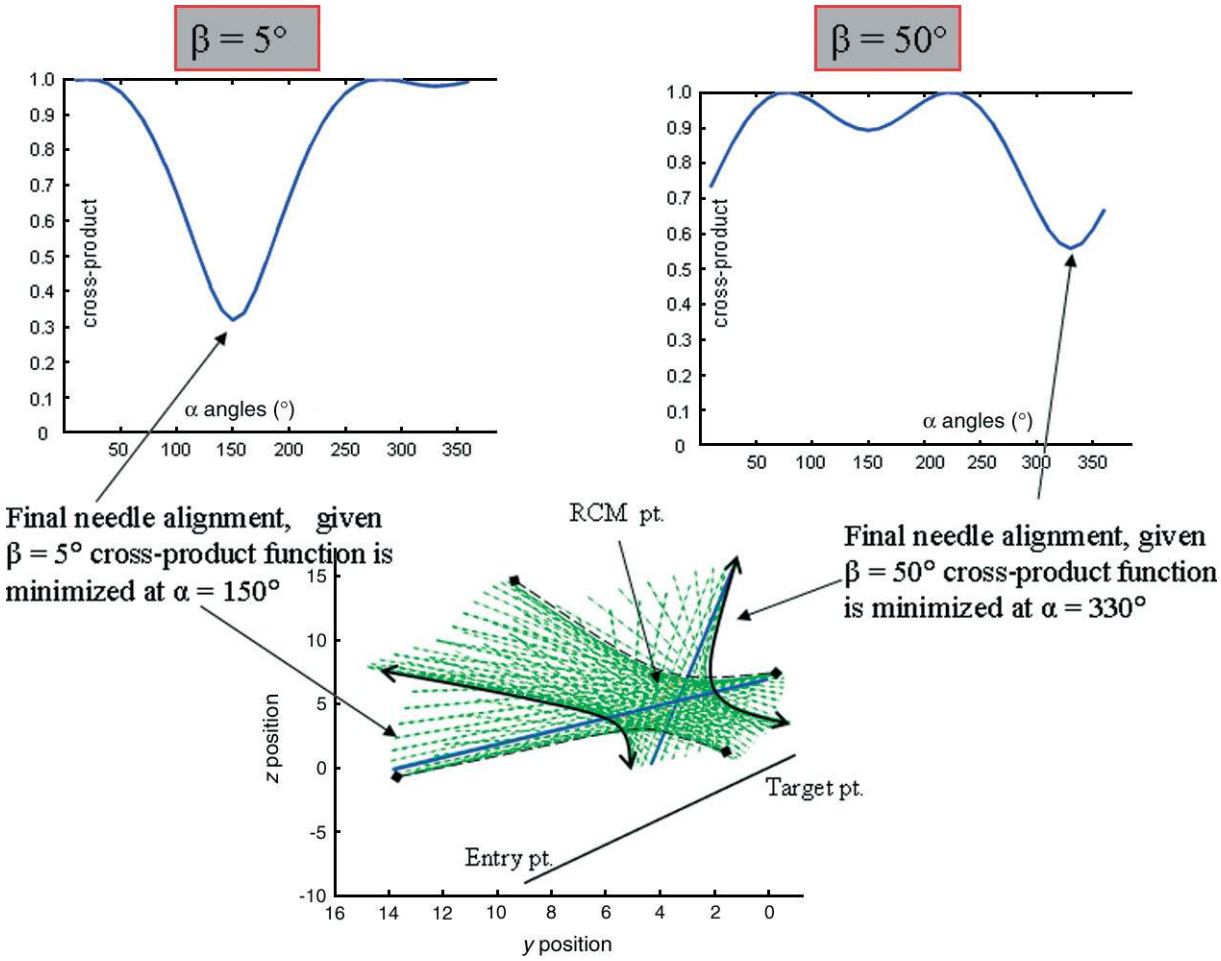

Figure 3. Shown here (bottom image) are 360 incremental rotations of α for two particular β angles (needle positions shown in green, dashed lines). This illustrates the dependency between α and β that arises when the needle tip is not placed at a mechanically constrained RCM point. Shown in blue solid lines are the closest possible alignments with the entry point-target point vector. A β of 5° offers better potential alignment (top left image) than a β of 50° (top right image), as illustrated by the lower minimum value of the cross-product heuristic with respect to α

options including voxel nearest neighbour (VNN) (31), pixel nearest neighbour (PNN) (32), distance-weighted (e.g. Shepard or Gaussian) methods (32) and radial basis functions (33). In the experiments presented in this paper, we applied PNN because it is not computationally intensive and does not degrade the quality of reconstruction.

- The *processing and visualization module*, which enhances the US images by applying smoothing, anisotropic diffusion and/or morphological operators. The specific algorithm applied is user-selectable and we applied Gaussian smoothing in the experiments presented in this paper.
- The *calibration module*, which performs spatial calibration to and transforms image data from the US image frame to the tracker coordinate system.

Two calibration processes are central to the accuracy of the 3D US system – temporal calibration and spatial calibration. Temporal calibration involves estimating the latencies between the tracking device and the video signal from the US machine. The goal is to synchronize both streams. One process acquires US images and places them in reserved memory, while another acquires readings from the tracker and stacks them in memory. Synchronization calibration is performed once per hardware/software configuration.

One method for temporal calibration was originally introduced in Stradx (19) and involves creating a coincident feature in both information streams. A sudden movement of the US probe (5–10 cm in <100–200 ms) accomplishes this, and careful examination of both streams enables a latency estimate. One drawback of this method is the reliance on qualitative observation of the US stream by the human operator to identify the time of the motion.

To provide a calibration method that does not rely on observation of US images, we developed a novel hardware-based calibration procedure (34). This involved using assembly code to output a logical signal within four to six machine cycles of the time image acquisition is commanded to the US machine. A second logical signal is similarly output at the time the tracker reading is acquired. Viewing these signals on an oscilloscope enables adjustment of a hard-coded delay, such that the

DOI: 10.1002/rcs

tracker reading is commanded at the mid-point of the US image acquisition time. The delay is repeatable and predictable, provided that the computer operating system is not tasked with superfluous additional processes (e.g. Internet Explorer, Visual C++ development environment, etc.) during the experiment.

The spatial calibration process involves determining the six-DOF rigid body transformation between the position of the magnetic tracking sensor attached to the US handle, and the image frame of the B-mode US. The scale factors in both x and y directions between pixels and physical dimensions must also be computed. Spatial calibration is usually performed by scanning and reconstructing a known object. The discrepancy between the reconstructed shape and the known shape then enables a re-estimation of calibration parameters. Once the transformation to the image frame is determined and the scale factors are known, one can place every pixel in the image coordinate system into the 3D US reconstruction space. We have accomplished this spatial calibration process using techniques ranging from conventional offline phantom-based methods (35) to real-time phantomless patient-specific calibration methods (36). In this paper we used the Hopkins method (37).

While using a commercial 3D US probe might initially seem preferable to reconstructing a 3D volume from tracked 2D US images, there are a number of drawbacks in doing so. First, the 3D US probe would not simplify the complete system, because it would still require a magnetic tracker attached to the probe handle, along with spatial and temporal calibration procedures similar to (and potentially more complex than) those described above. Further, 3D US probes are more bulky (limiting manoeuvrability within the patient) and expensive than 2D US probes, and not as widely available. Also, the frequency of 3D volumes returned for given US quality settings would likely be comparable to those achieved by compounding tracked 2D US images into a 3D volume. These factors motivate the use of tracked freehand 3D US built from 2D US images, rather than a commercial 3D US probe, for IGT applications such as ours.

Integration, planning and visualization software

For our graphical user interface, and to control our robot, we adapted the 3D Slicer medical data visualization package (38). This is a public domain, open source system, primarily developed by the Surgical Planning Laboratory at the Brigham and Women's Hospital (45), with sustained contribution from our group. We enhanced Slicer with a generic 3D US processing module, providing synchronized real-time capture of 2D US data and position information, and robust assembly of a spatially registered 3D volume from sparse and irregular 2D information. The software also provides a customizable real-time overlay display of the US volume, the needle tip with its current ablating range, and the current 2D US slice. Tumour coverage can be planned with single-spot or overlapping multiple ablations. In addition to the visual overlay, other visual and metric tools provide additional information to the operator. The system reports the current insertion depth, which can be compared against a ruler on a passive insertion stage as a redundant safety measure. The system also reports the distance between the actual and planned radiofrequency ablator tip position, and provides coordinate systems and landmarks to ease navigation in the virtual space, as shown in Figure 4.

Low-level control of the robot is achieved using a motion control card (MEI Inc.), driven with the Modular Robot Control library (39). The readings of the FOB tracker are reported to the workstation running 3D Slicer. As mentioned earlier, Slicer hosts three different programmes/modules simultaneously. These include the robot control interface, the 3D US module (CISUS) and the planning and visualization interface (Figure 5).

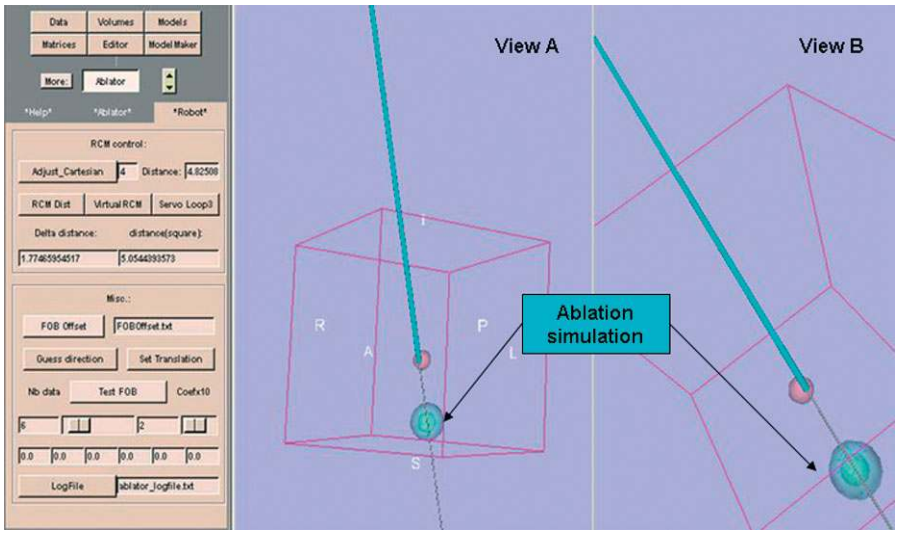

Figure 4. The software user interface window, showing two views of a 3D planning and visualization environment based on 3D Slicer

DOI: 10.1002/rcs

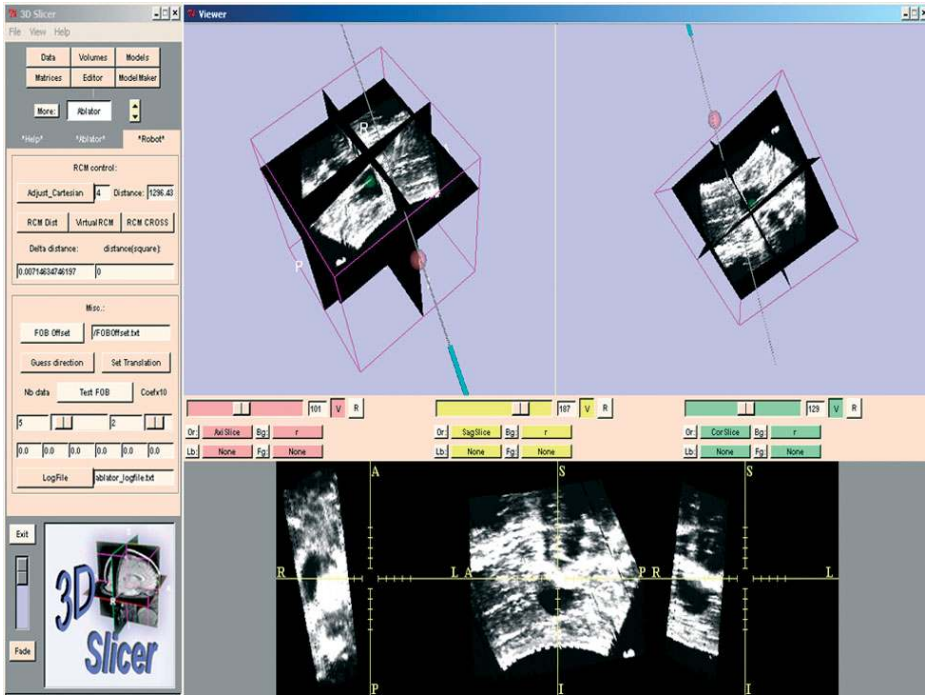

Figure 5. The CISUS interface under the 3D Slicer. The tracked 3D US volume collected in real tissue is shown from two different angles and in the bottom pane are three 2D sections. The needle location is shown in real time as a thick cylinder registered to the US volume, with the thin line emanating from it showing a straight, forward trajectory. There are two overlaid spheres, one for selecting a planned insertion point, and the other for selecting a planned target. The targeting sphere is centred at the lesion. Note that the quality of the freehand tracked 3D US volume is sufficient for image guidance, and arbitrary slices of it have the apparent quality of normal B-mode US images

Experiments

The experiments described in this section are designed to compare the 3D US image-guided robotic needle placement system described above with the current clinical gold standard for needle placement: manual needle manipulation based on manual 2D US guidance. We conducted two sets of experiments, one to assess the baseline accuracy of the system using *ex vivo* bovine liver tissue, and a second in a live animal (porcine) model. These results follow several previously published synthetic phantom tissue and *ex vivo* animal tissue experiments, which demonstrated the accuracy of the components of our system independently. Experiments validating the robotic component and control algorithm independent of imaging are reported in (7), where the system achieved angular accuracy of $<2°$, even in the worst-case trial where the needle began far from the correct alignment. Experiments evaluating the 3D US components independent of a robot are reported in (28), where phantom experiments were conducted to adequately observe and manually target a sphere in a water bath with a needle. We also performed previous experiments with the fully integrated 3D US-guided robotic system, in which we evaluated only success/failure (rather than quantitative accuracy, as we do here) of hitting simulated lesions embedded in bovine liver. The successful hit rate was 100% for seven simulated lesions at depths ranging from 5 to 40 mm (5). In this paper, we compare the system's quantitative accuracy and repeatability (rather than simply hit/miss rate) experimentally with current clinical gold-standard manual technique.

Our first set of experiments evaluated accuracy and repeatability in *ex vivo* bovine liver. Three lesions were embedded in the liver as targets (artificial tumours). These lesions were composed of 2% agar, 7% alcohol, 20% contrast agent and 71% distilled water by volume, a composition which ensures visibility under both US and X-ray imaging (see Figure 5 and 7). Note that this composition also made the simulated lesions robust to multiple needle insertions. The lesions were retrieved and inspected at the conclusion of the experiments and found to be intact and in their initial spherical shapes, despite multiple needle punctures. The three lesions were placed at varying depths within the liver. A shallow lesion (diameter 34 mm) was placed 3 cm below the surface, and two deep lesions (diameters 22 and 34 mm, respectively) were placed at depths of 8 and 14 cm.

A second set of experiments evaluated needle placement in a live animal (porcine) model, as shown in Figure 9. A simulated lesion of the same composition as above was implanted using a balloon catheter inserted through the liver surface in the manner of a needle (rather than intravascularly). The simulated lesion was deposited by using the lesion material in liquid form to inflate the balloon. The lesion material then rapidly solidified and the catheter balloon was removed by puncturing it with a needle. The catheter was then withdrawn, leaving the simulated lesion in place.

DOI: 10.1002/rcs

For data collection we used both US and an encoded C-arm fluoroscope. Fluoroscopy was included (rather than US alone) to provide independent measurements and to collect coronal projections. In surgery, the US probe cannot be arbitrarily orientated, due to limited space within the body, making the coronal projection challenging (and often impossible) to collect. This is one motivation for the use of 3D US imaging. The fluoroscope (Figure 7) provides accurate 3D measurements (coronal and sagittal projections collected) and provides a means of independently assessing the accuracy of tip placement and validating our system.

Using this experimental set-up, we tested accuracy, repeatability and the hypothesis that planning based on 2D US data lacking coronal projections could suffer from biased targeting error, with larger errors in the non-viewed coronal projection. To test this hypothesis, we compared manual needle tip targeting accuracy in the coronal and sagittal projections with the accuracy of our tracked 3D US system in the same projections.

The experimental procedural workflow of 3D US-guided robotic needle insertion is as follows:

1. *Exploration.* Manually scan the US probe over the liver surface to identify the approximate volume of interest (VOI) containing target lesions.
2. *Volume scanning.* After identifying the VOI, scan it with one simple translational sweep across the organ surface, while capturing continuous streams of temporally correlated US images and tracking data. The 2D US images are then compounded into a 3D US volume as described above. Figure 6 depicts three orthogonal slices of an example 3D US volume.
3. *Planning.* Use the interactive 3D Slicer interface to identify target and entry points. The visual onscreen display shows the trajectory of the needle and the predicted region of ablation. The computer also displays the planned and estimated current insertion depth of the needle.
4. *Robot motion.* Attach a depth marker to the needle shaft at the appropriate distance from the tip, and place the needle into the needle guide on the robot. The robot then translates and aligns the needle using virtual RCM control, as follows: (a) orientate the needle approximately; (b) move the needle tip to the entry point; and (c) further fine-tune the alignment as described in (7).
5. *Insertion.* Manually insert the needle through the guide to the predetermined depth, while monitoring both the physical depth marker and the real-time onscreen depth display.
6. *Assessment.* Use the C-arm to capture coronal and sagittal projections with the needle in place. These images are then analysed by measuring the distance between the needle tip and the centre of the lesion.

The details of the procedural workflow in the manual 2D US-guided procedure are somewhat dependent on the individual physician's style, but it consists of the following general steps:

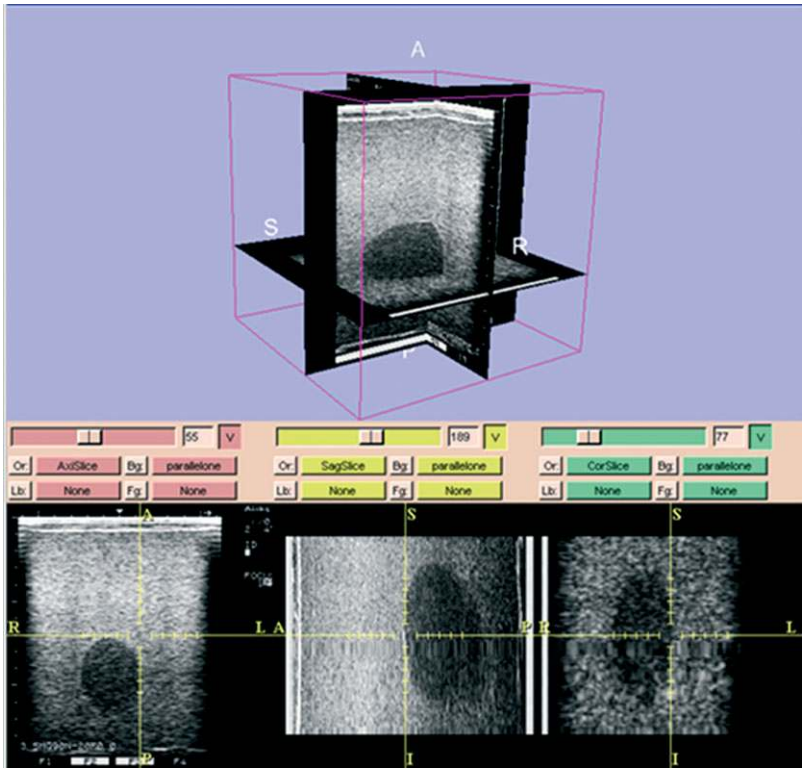

Figure 6. A larger view of a 3D US reconstruction similar to that found in Figure 5. This volume was collected in phantom tissue and an embedded synthetic lesion is evident. The bottom three images show 2D slices through the 3D volume

DOI: 10.1002/rcs

1. *Exploration.* Manually scan the US probe over the liver surface to identify the approximate VOI containing target lesions.
2. *Volume scanning.* After identifying the VOI, scan it several times with the 2D US to construct a mental 3D understanding of tumour size, shape and surrounding structures.
3. *Planning.* Mentally determine a desired entry trajectory.
4. *Needle/US manipulation and insertion.* With the US probe in one hand and the needle in the other, insert the needle, attempting to hit the desired target. Manually manipulate US probe position and orientation as desired to visualize the needle and target during insertion.
5. *Assessment.* Scan the VOI again after the needle is in place and make a qualitative judgement on whether accuracy is sufficient. If not, remove and reinsert the needle. When desired tip position is achieved, the C-arm captures data as described in step 6 of the image-guided robotic procedure above. Importantly, the operator's decision on whether sufficient accuracy had been achieved was based on 2D US images only. Both the 3D US and X-ray images were hidden from the operator during insertions.

For each trial in our experiments, we used one insertion with the image-guided robotic system and up to six insertions with the manual 2D US protocol. Clinically, using the manual procedure, several insertions are often performed to achieve the desired tip position accuracy. It has been noted by one study that approximately five insertions were required manually to hit a lesion 3 mm in diameter, with 95% confidence in manual needle insertions under 3D US (18). In the manual procedure in our experiments, the surgeon was allowed to remove and reinsert the needle until satisfied with the accuracy of tip position, or the maximum of six trial insertions had been completed. A single insertion was defined as motion of the needle into tissue without retraction. Changing the US probe angle and/or tilting the needle were not considered to signal the start of a new insertion. The end of the insertion was considered to be the point at which the operator began to withdraw the needle from the tissue.

Results and Discussion

In the first set of experiments in *ex vivo* bovine liver, nine needle placement trials (with up to six insertions per trial) were collected using the manual 2D US protocol, and six needle placement trials (with one insertion per trial) were collected using the robotic system. We then compared the targeting accuracy of the first insertion (generally the least accurate) and last insertion (generally the most accurate) of the manual case with the single trial of the image-guided robotic system (Figure 8). As shown in the figure, error components in the coronal projection are substantially larger than those of sagittal projection for the first trial of the manual procedure ($p < 0.05$). However, using the robotic system, error components are comparable in both projections and substantially lower than those of the first trial of the manual insertion ($p < 0.05$). Allowing the operator remove and reinsert the needle up to six times (three was average), reduces the average error components in both projections. The average errors of the 3D US system in both projections remain lower than those of the last trial of the freehand procedure, but the differences were not statistically significant.

Repeatability of needle placement is also an important metric, and can be evaluated by examining the standard deviation (SD) of tip placement accuracy. In our experiments, the image-guided robotic system had a projection SD of 1.56 mm, compared to 3.19 and 4.63 mm for the first and last manual insertions, respectively. A higher number of insertions increases the invasiveness of a manual trial. As mentioned previously, several insertions are generally required to achieve desired manual accuracy. For the shallow lesion, satisfactory positioning generally required only one or two insertions. For the smaller of the deep lesions, located 8 cm below the surface, the maximum six insertions were often required.

Our second set of experiments evaluated needle targeting accuracy with the additional complications present in the live animal case (Figure 9). Two insertions were performed with the image-guided robotic system. The first missed the planned target (centre of the lesion) by more than 1 cm. This was primarily due to organ and lesion motion resulting from respiratory effects. In the second trial, we used respiratory control by the anaesthesiologist to reduce breathing frequency. The system was then able to acquire US, plan, and insert the needle within 20 s with 5.5 mm overall tip accuracy. This experiment illustrates the additional challenges involved in the *in vivo* needle placement, viz. compensating for the target motions and deformations that occur in real surgery.

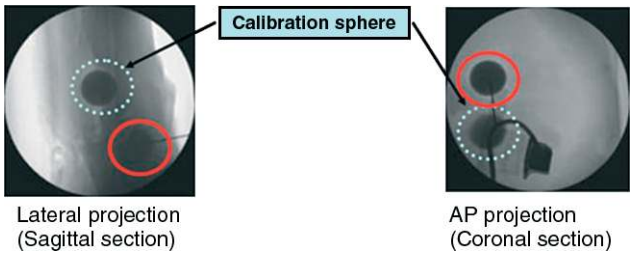

Figure 7. These two perpendicular X-ray projections show an example of a needle embedded in a simulated lesion (sphere inside solid red circle) and a calibration sphere (circled with a dashed line). The calibration sphere is not involved in the experiment, but was placed in the image to provide an object of known reference geometry for calibrating the C-arm. The dark square with trailing wire in the right image is the magnetic tracker attached to the needle holder. The needle holder itself was radiolucent and so does not appear in the images

DOI: 10.1002/rcs

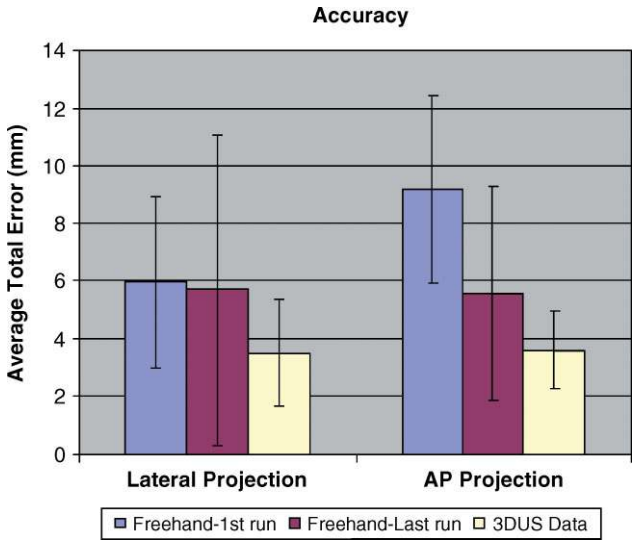

Figure 8. A comparison of average targeting accuracy for manual freehand 2D US needle insertion and robotic 3D US needle insertion, in the lateral (or sagittal) projection and anterior–posterior (or coronal) projection. Error bars indicate SD

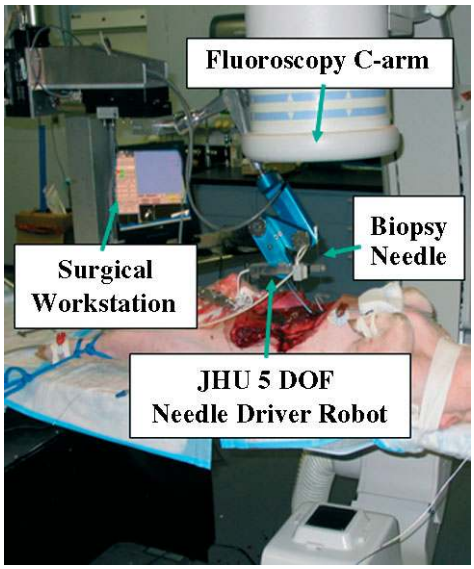

Figure 9. The 3D US-guided robotic needle placement system, as arranged for *in vivo* experiments with fluoroscopy to assess the targeting accuracy. Note that, in the above image, the C-arm is orientated to acquire the coronal projection, which can be difficult or impossible to acquire manually with 2D US, due to workspace constraints from patient anatomy

Conclusions and Future Work

The results of these experiments with 3D US image-guided robotic needle placement indicate that such enabling technologies hold the promise to enhance the accuracy and repeatability of needle placement in many types of intervention, including ablative therapy in the liver. Our results also illustrate that it is important to consider error bias with manual 2D US needle placement, which can lead to larger errors in the coronal plane, particularly during the first insertion. We propose that 3D US is a solution to this error bias, since our image-guided robotic system showed no error bias. It may be that the presentation of 3D US data to the operator alone (without a robot) would be sufficient to reduce this bias, but demonstrating this is a topic of future work.

One benefit that is clear when using an image-guided robotic system is an increase in repeatability and thus a reduction in invasiveness, because fewer insertions are required for accurate tip placement. As we have noted, it is often necessary to make multiple insertions in clinical practice – especially when targeting deep lesions. The necessity of multiple insertions has been corroborated by other published results, notably (18), discussed previously, where experiments assessed manual needle insertion under 3D US. The authors of that study used several simulated lesion sizes and assessed only whether the tip of the needle had penetrated the lesion. They found that for the specific depths and US parameter settings they used, success could only be guaranteed for lesions of 10 mm diameter or more, while lesions 3 mm in diameter had a success rate of only about 50%.

In our experiments, the single insertion accuracy and consistency of the image-guided robot suggest that a robot can improve some aspects of needle placement, including reducing the number of insertions necessary. However, it is worth noting that the operator's accuracy actually slightly exceeded that of the image-guided robotic system in targeting the easier, shallow lesion. However, the image-guided robotic system consistently produced similar accuracy and repeatability results regardless of lesion depth, whereas deeper lesions were significantly more challenging for human operators.

It is difficult to determine the extent to which the benefits of our image-guided robotic system are due to 3D US or to robotic needle manipulation. However, the repeatability of the system does appear to be primarily a consequence of the robot. We believe that 3D US will be particularly useful in planning and visualization of the lesion in comparison to sensitive surrounding structures, although the experiments presented here were not designed to investigate planning, and we leave planning under 3D US to future work.

The accuracy of the image-guided robotic system is mainly dictated by the accuracy of the tracking system and the calibration procedures. The tracker used in our experiments was a first-generation magnetic tracker with an RMS accuracy of 2.54 mm. Use of more accurate magnetic or optical tracking (e.g. the Polaris optical tracker from NDI Inc.) is expected to enhance overall system accuracy. However, there is a cost trade-off in doing so, since optical tracking systems are often more expensive and more cumbersome to deploy clinically than their magnetic counterparts. It appears that magnetic tracking will be a sufficiently accurate long-term solution for systems like ours. For example, magnetically tracked manual needle insertion guided by preoperative CT alone has been shown clinically feasible (40). The more

important immediate improvements necessary in our system were illustrated by the *in vivo* experiment.

In the *in vivo* animal experiment, complications arose regarding motion artifacts and needle bending. One way of compensating for these effects is closed-loop control of steerable needles. Toward this end, we have been developing bevel-steered needles, which harness the natural bending forces that arise from a standard bevel tip to create controllable deflection. Webster *et al*. modelled the kinematics of steerable needles (41), and several research groups have demonstrated promising recent results in model-based image-guided closed-loop control and planning, the results of which are surveyed in (42). Alternative steering techniques based on precurved concentric tubes have also been recently developed, with the potential to control the path of the cannula through tissue by telescopic extension and axial component tube rotation, which actively changes cannula shape (42,43).

Another future research direction involves quantifying manual needle alignment accuracy to determine how well humans manipulate needles. This study will employ several expert surgeons, as well as several novice surgeons, to determine average manual accuracy under both 3D US and 2D US imaging. It will also allow us to more fully define the effects of 3D US imaging compared with the robotic component in our system. The experimental procedure may be structured in a manner similar to the experiments presented in (18), but we intend to assess accuracy and consistency directly, using a C-arm, rather than collecting binary hit/miss data only. Further, we also plan to evaluate human pre-insertion alignment directly, apart from post-insertion targeting accuracy, so that a more direct comparison between human and robot alignment ability is possible. This will help to quantify the amount of 'steering' human operators apply by hand in the form of forces and torques at the base of the needle during insertion. This can be assessed apart from 3D US, using tracking or calibrated optical cameras to determine how closely subjects have aligned the needle with a separately presented desired entry vector shown to them.

We also plan to pursue multi-modal image registration to augment the US images with preoperative CT/MRI data when they are available (44). For example, sometimes when chemotherapy is administered before surgery, tumours can disappear from view in a given single imaging modality. In this case, augmenting 3D US data with information from preoperative CT can reveal the tumour location. In all such future studies, it will be important to consider the speed of data collection and the algorithms used to process the data, so that the system can compensate (either by needle steering, or robotic needle base servoing) for tissue motion due to heartbeat and respiratory effects.

Acknowledgements

The authors would like to acknowledge the intellectual contribution of Gabor Fichtinger (Queen's University, Canada) to the work described herein. They would also like to thank Michael Awad, Michelle de Oliveira and Carolyn McGee for assistance with animal and *ex vivo* experiments, and Anand Viswanathan for assistance with data collection and system programming. Financial support for this work was provided by the NIH under STTR 5-1R41CA103468-01, the NSF under CISST/ERC EEC9731748 and an NDSEG graduate fellowship. This research followed protocols approved by relevant accredited ethical committees at Johns Hopkins University.

References

1. Wood TF, Rose DM, Chung M, *et al*. Radiofrequency ablation of 231 unresectable hepatic tumors: indications, limitations, and complications. *Ann Surg Oncol* 2000; **7**(8): 593–600.
2. Loser MH, Navab N. A new robotic system for visually controlled percutaneous interventions under CT fluoroscopy. *Lect Notes Comput Sci* 2000; **1935**: 887–896.
3. Cleary K, Nguyen C. State of the art in surgical robotics: clinical applications and technology challenges. *Comp Aided Surg* 2002; **6**(6): 312–328.
4. Boctor EM, Webster RJ III, Mathieu H, *et al*. Virtual remote center of motion control for needle placement robots. Sixth International Conference on Medical Image Computing and Computer-Assisted Intervention. *Lect Notes Comput Sci* 2003; **2878**: 157–165.
5. Boctor EM, Webster RJ III, Taylor RH, *et al*. Robotically assisted ablative treatment guided by freehand 3D ultrasound. *Proceedings of Conference of Computer Assisted Radiology and Surgery (CARS), Chicago, 2004*. Elsevier: New York, 2004; 503–508.
6. Boctor EM, Fischer G, Choti M, *et al*. Dual-armed robotic system for intraoperative ultrasound guided hepatic ablative therapy: a prospective study. Proceedings of IEEE International Conference on Robotics and Automation, 2004; 377–382.
7. Boctor EM, Webster RJ III, Mathieu H, *et al*. Virtual remote center of motion control for needle placement robots. *J Comput Assist Surg* 2004; **9**(5): 175–183.
8. Yu AS, Keeffe EB. Management of hepatocellular carcinoma. *Rev Gastroenterol Disord* 2003; **3**(1): 8–24.
9. Bruix J, Sherman M. Management of hepatocellular carcinoma. *Hepatology* 2005; **42**(5): 1208–1236.
10. Lencioni R, Crocetti L. Radiofrequency ablation of liver cancer. *Tech Vasc Interv Radiol* 2007; **10**(1): 38–46.
11. Kuszyk BS, Boitnott JK, Choti MA, *et al*. Local tumor recurrence following hepatic cryoablation: radiologic–histopathologic correlation in a rabbit model. *Radiology* 2000; **217**(2): 477–486.
12. Koniaris LG, Chan DY, Magee C, *et al*. Focal hepatic ablation using interstitial photon radiation energy. *J Am Coll Surg* 2000; **191**(2): 164–174.
13. Choti MA. Hepatic radiofrequency ablation. *Cancer J* 2000; **6**(4): 291–292.
14. Choti MA. Surgical management of hepatocellular carcinoma: resection and ablation. *J Vasc Interv Radiol* 2002; **13**(9, suppl): S197–203.
15. Izumi N, Asahina Y, Noguchi O, *et al*. Risk factors for distant recurrence of hepatocellular carcinoma in the liver after complete coagulation by microwave or radiofrequency ablation. *Cancer* 2001; **91**(5): 949–956.
16. Daum DR, Smith N, McDannald N, *et al*. MR-guided noninvasive thermal coagulation of *in vivo* liver tissue using ultrasonic phased array. *Thermal Treatment of Tissue with Image Guidance*, Ryan T, Wong TR (eds). Proceedings of SPIE, 1999; 185–195.
17. Haar G. Ultrasound focal beam surgery. *Ultrasound Med Biol* 1995; **21**(9): 1089–1100.
18. Fenster A, Downey DB, Cardinal NH. Three-dimensional ultrasound imaging. *Phys Med Biol* 2001; **46**: 67–99.
19. Prager RW, Gee AH, Berman L. Stradx : real-time acquisition and visualization of freehand three-dimensional ultrasound. *Med Image Anal* 1999; **3**(2): 129–140.
20. Sakas G. *In vivo* interactive visualizer of large scalar voxel fields. *Comput Graphic Topics* 1992; **4**(2): 12–13.
21. Burdette EC, Holupka EJ, Kaplan IR. Virtual reality 3D visualization for surgical procedures. US Patent No. 6 256 529: issued 3 July 2001, filed 24 November 1997.

22. Burdette EC, Komadina B. Real-time brachytherapy spatial registration and visualization system. US Patent No. 6 129 670: issued: 10 October 2000, filed 29 May 1998.
23. Doggett SJ, Burdette EC. Intraoperative treatment planning for prostate brachytherapy. Proceedings of the Annual Meeting of the American Brachytherapy Society, Washington, DC, May 2000.
24. Computerized Medical Systems (CMS), St. Louis, MO, USA: http://www.cms-stl.com.
25. Varian Medical Systems, Palo Alto, CA, USA: http://www.varian.com.
26. Boctor EM, Viswanathan A, Pieper S, *et al*. CISUS: an integrated 3D ultrasound system for IGT with modular tracking interface. Annual Conference of the International Society for Optical Engineering (SPIE) on Medical Imaging. *Proc SPIE* 2004; **5367**: 247–256.
27. Kon R, Leven J, Kothapalli K, *et al*. CIS-UltraCal: an open-source ultrasound calibration toolkit. SPIE Medical Imaging 2005: Ultrasonic Imaging and Signal Processing, Walker WF, Emelianov SY (eds). *Proc SPIE* 2005; **5750**: 516–523.
28. Boctor EM, Fichtinger G, Taylor RH, *et al*. Tracked 3D ultrasound in radio-frequency liver ablation. Annual Conference of the International Society for Optical Engineering (SPIE) on Medical Imaging Ultrasonic Imaging and Signal Processing, Walker WF, Insana MF (eds). *Proc SPIE* 2003; **5035**: 174–182.
29. Stoianovici D. URobotics – urology robotics at Johns Hopkins. *Comput Aid Surg* 2001; **6**: 360–369.
30. Susil RC, Anderson JH, Taylor RH. A single image registration method for CT-guided interventions, MICCAI. *Lect Notes Comput Sci* 1999; **1679**: 798–808.
31. Sherebrin S, Fenster A, Rankin RN, *et al*. Freehand three-dimensional ultrasound: implementation and applications. Medical Imaging 1996: Physics of Medical Imaging, April 1996, Van Metter RL, Beutel J (eds). *Proc. SPIE* 1996; **2708**: 296–303.
32. Barry CD, Allott CP, John NW, *et al*. Three-dimensional freehand ultrasound: image reconstruction and volume analysis. *Ultrasound Med Biol* 1997; **23**(8): 1209–1224.
33. Rohling R, Gee AH, Berman LH, *et al*. Radial basis function interpolation for freehand 3D ultrasound. In *Information Processing in Medical Imaging*, Kuba A, Samal M, Todd-Pokropek A (eds). *Lecture Notes in Computer Science*, vol 1613. Springer: Berlin, 1999; 478–483.
34. Boctor EM. Enabling Technologies for Ultrasound Imaging in Computer-assisted Intervention. PhD Thesis, Department of Computer Science, Johns Hopkins University, Baltimore, MD, 2006.
35. Boctor EM, Viswanathan A, Choti MA, *et al*. A novel closed form solution for ultrasound calibration. In IEEE International Symposium on Biomedical Imaging, 2004; 527–530.
36. Boctor EM, Iordachita I, Fichtinger G, *et al*. Ultrasound self-calibration. Medical Imaging 2006: Visualization, Image-guided Procedures and Display, Cleary KR, Galloway RL Jr (eds). *Proc SPIE* 2006; **6141**: 784–795.
37. Boctor EM, Jain A, Choti MA, *et al*. Rapid calibration method for registration and 3D tracking of ultrasound images using spatial localizer. Medical Imaging 2003. *Proc SPIE* 2003; **5035**: 521–532.
38. Gering DT, Nabavi A, Kikinis R, *et al*. An integrated visualization system for surgical planning and guidance using image fusion and an open MR. *J Magn Reson Imaging* 2001; **13**(6): 967–975.
39. Taylor RH, Kumar R, *et al*. Library of Modular Robots Control, Engineering Research Center Computer Integrated Surgical Systems and Technology: http://www.cisst.org/resources/software/mrc/ [accessed 16 January 2003].
40. Banovac F, Tang J, Xu S, *et al*. Precision targeting of liver lesions using a novel electromagnetic navigation device in physiologic phantom and swine. *Med Phys* 2005; **32**(8): 2698–2705.
41. Webster RJ III, Cowan NJ, Chirikjian GS, *et al*. Nonholonomic modeling of needle steering. *Int J Robotics Res* 2006; **25**(5/6): 509–526.
42. Webster RJ III. Design and Mechanics of Continuum Robots for Surgery. PhD Thesis, Department of Mechanical Engineering, Johns Hopkins University, Baltimore, MD, 2007.
43. Webster RJ III, Okamura AM, Cowan NJ. Toward active cannulas: miniature snake-like surgical robots. IEEE/RSJ International Conference on Intelligent Robots and Systems (IROS), Beijing, China, 9–15 October 2006; 2857–2863.
44. Wein W, Khamene A, Clevert D, *et al*. Simulation and fully automatic multimodal registration of medical ultrasound. Medical Image Computing and Computer-Assisted Intervention – MICCAI (1), 2007; Brisbane, Australia.
45. MIT AI Lab and the Surgical Planning Lab at Brigham & Women's Hospital: http://www.slicer.org.
46. Centre for Medicine and Technology (MISON), Norway: http://www.mison.no.
47. National Cancer Institute (NCI), Surveillance Epidemiology and End Results (SEER), providing information on cancer statistics on the US population: http://seer.cancer.gov.